

Ultrahard BC₅ - an efficient nanoscale heat conductor through dominant contribution of optical phonons

*Rajmohan Muthaiah¹, Jivtesh Garg¹, Shamsul Arafin²

¹School of Aerospace and Mechanical Engineering, University of Oklahoma, Norman, OK-73019, USA

²Department of Electrical and Computer Engineering, Ohio State University, Columbus, OH-43210, USA

Abstract: In this work, we study thermal conductivity (k) of BC₅, an ultra-hard diamondlike semiconductor material, using first-principles computations and analyze the effect of both isotopic disorder as well as length scale dependence. k of isotopically pure BC₅ is computed to be 169 Wm⁻¹K⁻¹ (along a-axis) at 300K; this high k is found to be due to the high frequencies and phonon group velocities of both acoustic and optical phonons owing to the light atomic mass of Carbon (C) and Boron (B) atoms and strong C-C and B-C bonds. We also observe a dominance of optical phonons (~ 54%) over acoustic phonons in heat conduction at higher temperatures (~500 K). This unusually high contribution of optical phonons is found to be due to a unique effect in BC₅ related to a weaker temperature dependence of optical phonon scattering rates relative to acoustic phonons. The effect is explained in terms of high frequencies of optical phonons causing decay into other high frequency phonons, where low phonon populations cause the decay term to become insensitive to temperature. The effect further leads to high nanoscale thermal conductivity of 77 Wm⁻¹K⁻¹ at 100 nm length scale due to optical phonon meanfreepaths being in nanometer regime. These results provide avenues for application of BC₅ in nanoscale thermal management.

Keywords: Boron, Carbon, thermal conductivity, optical phonons, BC₅, ultra-hard materials, thermal management, phonons, nanoelectronics

Introduction: Materials with high thermal conductivity are critical for efficient heat dissipation in power electronics and electronics cooling. Boron and carbon based compound-semiconductors are promising materials for thermal management due to their high thermal conductivity emerging from light mass of atoms involved and strong bonds of C-C and B-C¹⁻⁶. An ultra-high thermal conductivity of 2305 Wm⁻¹K⁻¹ for the super-hard bulk hexagonal BC₂N was reported by Safoura

*et al.*⁷. Similarly, high anisotropic thermal conductivities of 1275.79 Wm⁻¹K⁻¹ and 893.90 Wm⁻¹K⁻¹ were reported for monolayer BC₂N along zig-zag and arm-chair directions⁸. BC₅ is a diamond-like ultra-hard semiconductor with exceptional hardness of 83 GPa and experimental bulk modulus of 335 GPa^{9,10}. In this work we use first principles calculations to analyze the thermal conductivity of BC₅. At 300 K, we report a high thermal conductivity (k) of 169 Wm⁻¹K⁻¹ for bulk BC₅ (infinite dimensions) along a -axis. A high nanoscale thermal conductivity of ~ 51 Wm⁻¹K⁻¹ is reported for length scale of 50 nm (at 300 K), indicating BC₅ will be a promising material for thermal management in nanoelectronics. To understand the origin of this high nanoscale thermal conductivity we systematically analyzed elastic constants, phonon group velocities and phonon scattering rates of different phonon modes. The high nanoscale thermal conductivity is found to be due to a dominant contribution of optical phonons to overall thermal conductivity in BC₅; at 500 K and 1000 K, optical phonons (with meanfreepaths in the nanometer regime) contribute almost $\sim 54\%$ and 57.3% , respectively to the overall thermal conductivity along the a -axis. First-principles computations are used to shed light on the dominant role of optical phonons in BC₅ thermal conductivity.

Computational methods: First principles computations were performed using local density approximations¹¹ with norm-conserving pseudopotentials using QUANTUM ESPRESSO¹² package. The geometry of the tetragonal (space group P3m1) BC₅ with 6 atoms unit cell is optimized until the forces on all atoms are less than 10⁻⁵ eV Å⁻¹ and the energy difference is converged to 10⁻¹² Ry. A plane-wave cutoff energy of 100 Ry was used. Electronic calculations were performed using 12 x 12 x 6 Monkhorst-Pack¹³ k -point mesh. Optimized BC₅ structure is shown in Fig. 1; obtained lattice constants of $a=2.516$ Å and $c/a=2.506$ are in good agreement with the previous first principles calculations¹⁴. Elastic constants were computed using QUANTUM ESPRESSO thermo_pw package and Voigt-Reuss-Hill approximation¹⁵ is used to calculate the bulk modulus, shear modulus(G) and Young's

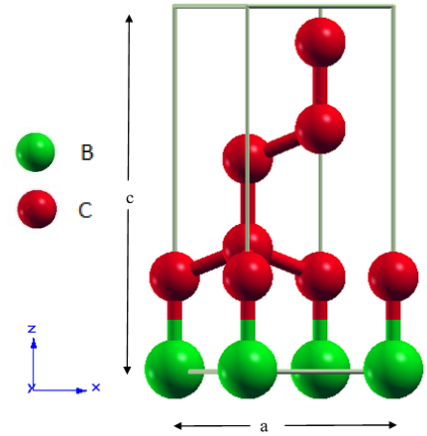


Figure 1: Atomic arrangements of BC₅ with space group P3m1. Red and green sphere represents the carbon and boron respectively.

Modulus(E). Lattice thermal conductivity is calculated by deriving the most important ingredients, namely, the harmonic and anharmonic interatomic force interactions from density-functional theory and using them with an exact solution of the phonon Boltzmann transport equation (PBTE)¹⁶⁻¹⁸. Thermal conductivity (k) in the single mode relaxation time (SMRT) approximation¹⁹ (usually the first iteration in solution of PBTE) is given by,

$$k_{\alpha} = \frac{\hbar^2}{N\Omega k_b T^2} \sum_{\lambda} v_{\alpha\lambda}^2 \omega_{\lambda}^2 \bar{n}_{\lambda} (\bar{n}_{\lambda} + 1) \tau_{\lambda} \quad (1)$$

where, $\alpha, \hbar, N, \Omega, k_b, T$, are the cartesian direction, Planck constant, size of the q mesh, unit cell volume, Boltzmann constant, and absolute temperature respectively. λ represents the vibrational mode (\mathbf{qj}) (\mathbf{q} is the wave vector and j represents phonon polarization). $\omega_{\lambda}, \bar{n}_{\lambda}$, and $v_{\alpha\lambda}$ ($= \partial\omega_{\lambda}/\partial q$) are the phonon frequency, equilibrium Bose-Einstein population and group velocity along cartesian direction α , respectively of a phonon mode λ . $\omega_{\lambda}, \bar{n}_{\lambda}$, and $c_{\alpha\lambda}$ are derived from the knowledge of phonon dispersion computed using 2nd order IFCs. τ_{λ} is the phonon and is computed using the following equation,

$$\frac{1}{\tau_{\lambda}} = \pi \sum_{\lambda'\lambda''} |V_3(-\lambda, \lambda', \lambda'')|^2 \times [2(n_{\lambda'} - n_{\lambda''})\delta(\omega(\lambda) + \omega(\lambda') - \omega(\lambda'')) + (1 + n_{\lambda'} + n_{\lambda''})\delta(\omega(\lambda) - \omega(\lambda') - \omega(\lambda''))] \quad (2)$$

where, $\frac{1}{\tau_{\lambda}}$ is the anharmonic scattering rate due to intrinsic three phonon interactions and $V_3(-\lambda, \lambda', \lambda'')$ are the three-phonon coupling matrix elements computed using both harmonic and anharmonic interatomic force constants. Dynamical matrix and harmonic force constants were calculated using 8 x 8 x 4 q-grid. 4 x 4 x 2 q-points were used to compute the anharmonic force constants using QUANTUM ESPRESSO D3Q^{16, 18, 20} package. Acoustic sum rules were imposed on both harmonic and anharmonic interatomic force constants. Phonon linewidth and lattice thermal conductivity were calculated iteratively using QUANTUM ESPRESSO thermal2 code with 30 x 30 x 15 \mathbf{q} -mesh and 0.05 cm⁻¹ smearing until the Δk values are converged to 1.0e⁻⁵. Casimir scattering²¹ is imposed for length dependence thermal conductivity calculations.

Results and discussions:

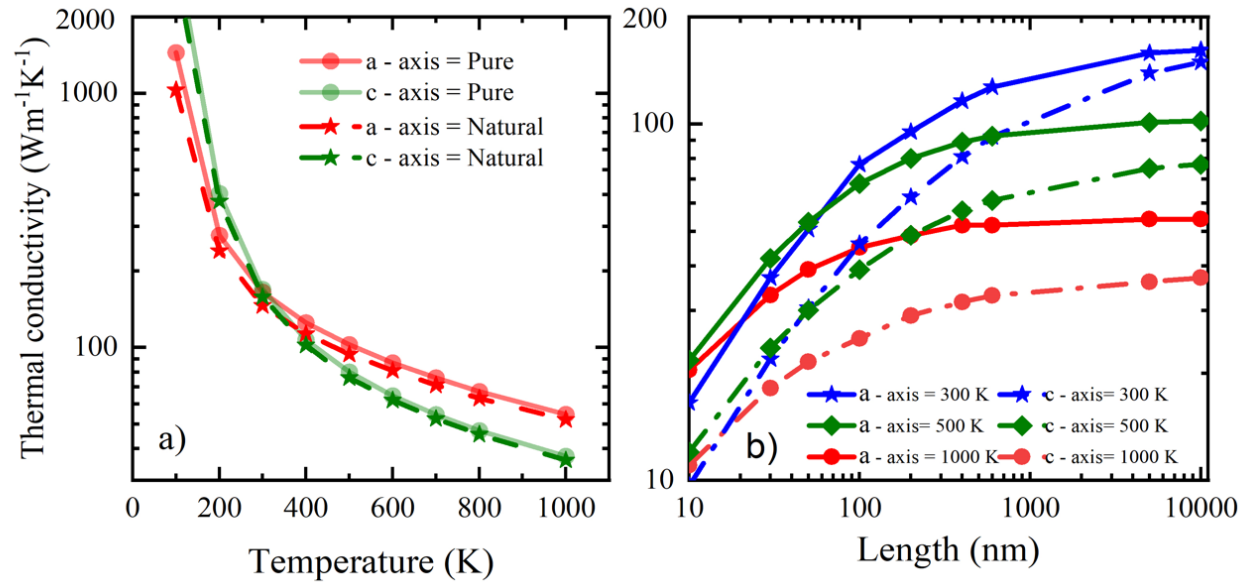


Figure 2: a) Thermal conductivity of BC₅ along a-axis and c-axis at different temperatures b) Length dependence of thermal conductivity (300 K) of BC₅ between 10 nm and 10000 nm.

Lattice thermal conductivity of isotopically pure and isotopically disordered (naturally occurring) BC₅ along a-axis and c-axis is shown in Fig 2a as a function of temperature. At room temperature (300 K), computed thermal conductivities of bulk BC₅ along a-axis and c-axis are 165 W/mK and 169 Wm⁻¹K⁻¹, respectively, for pure BC₅. Our reported k values are higher than the k values of silicon (153 Wm⁻¹K⁻¹)²² at room temperature suggesting that BC₅ will be a promising material for thermal management applications.

This high thermal conductivity of BC₅ is a direct consequence of high phonon frequencies and phonon group velocities in BC₅ as seen in Fig. 3 resulting from the strong C-C and B-C bonds, and the light mass of B and C atoms. While in silicon, the maximum LA phonon frequency reaches 400 cm⁻¹²³, Fig. 3 shows that in BC₅, LA phonons have higher frequencies, reaching values greater than 600 cm⁻¹. The strong bonding in BC₅ is seen by noticing that the bulk modulus and Young Modulus of BC₅ are higher than Silicon and almost equal to the values for Diamond (computations for Diamond and Silicon are discussed in supplementary section). This is due to the strong covalent bond network through sp^3 hybridization²⁴.

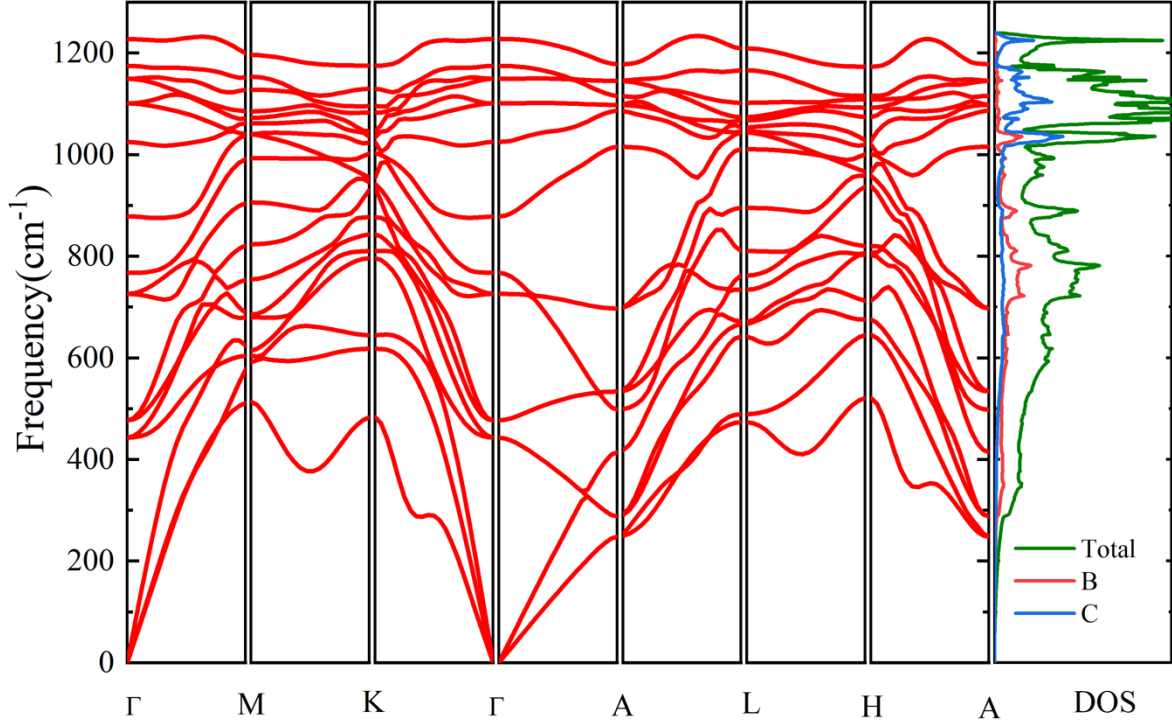


Figure 3: Phonon dispersion along the high symmetry points of tetragonal BC₅ and and phonon density of states

We also estimated k of naturally occurring BC₅ to be 146 W/mK and 158 Wm⁻¹K⁻¹, along a-axis and c-axis, respectively at 300 K. k of naturally occurring BC₅ is only lower by 11.5% and 6.5% relative to pure BC₅ along a-axis and c-axis respectively. Thermal conductivity for naturally occurring BC₅ was computed by introducing additional phonon scattering arising out of mass-disorder due to random distribution of isotopes of Boron and Carbon throughout the crystal. The small mass variation in isotopes of both B (atomic mass of 10.013 a.u with 19.9% concentration and atomic mass of 11.009 a.u with 80.1% concentration) and C (atomic mass of 12 a.u with 98.93% concentration and 13.003 a.u with 1.07% concentration) atoms²⁵, induces only a small additional phonon scattering, causing only a minor decrease in thermal conductivity of naturally occurring BC₅ relative to the pure case.

Table 1: Elastic constants of BC₅, Silicon and Diamond in GPa

Material	C11	C33	C44	C66	C12	C13	Bulk Modulus	Young modulus	Shear Modulus
BC ₅	911	1061.8	394.5	361.1	189	97	405	894	396

Silicon	159.5	159.5	78.1	78.1	61.3	61.3	94.1	158.1	64.8
Diamond	1099.5	1099.5	601.4	601.4	127.1	127.1	451.3	1176.8	552.3

Length dependent k of pure BC_5 was also investigated by introducing Casimir scattering (boundary

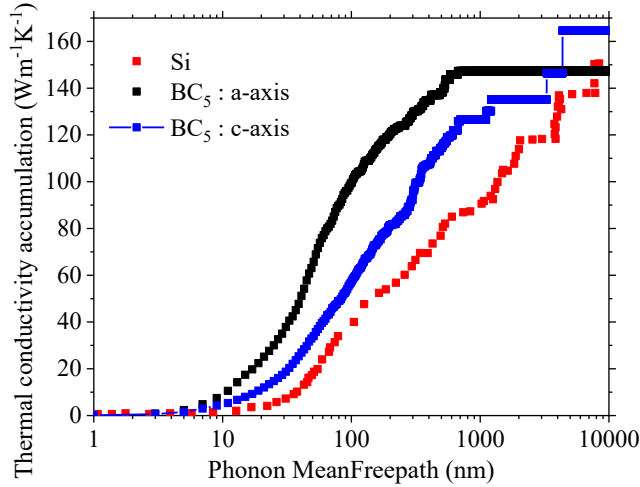


Figure 4: Phonon meanfreepath dependence thermal conductivity of BC5 and Silicon at 300

K

scattering). High thermal conductivity of $\sim 51 \text{ Wm}^{-1}\text{K}^{-1}$ at nanometer length scale of $L = 50 \text{ nm}$ (at 300 K) is observed in Fig. 2b. Nanoscale thermal conductivity of BC_5 is more than a factor of 2 higher than silicon as seen in Fig. 4 where we compare the phonon meanfreepath dependence of thermal conductivity accumulation in BC_5 and silicon. In silicon, phonons with meanfreepath below 100 nm contribute only $\sim 40 \text{ W/mK}$ at 300 K; in BC_5 , however, phonons in the same meanfreepath range,

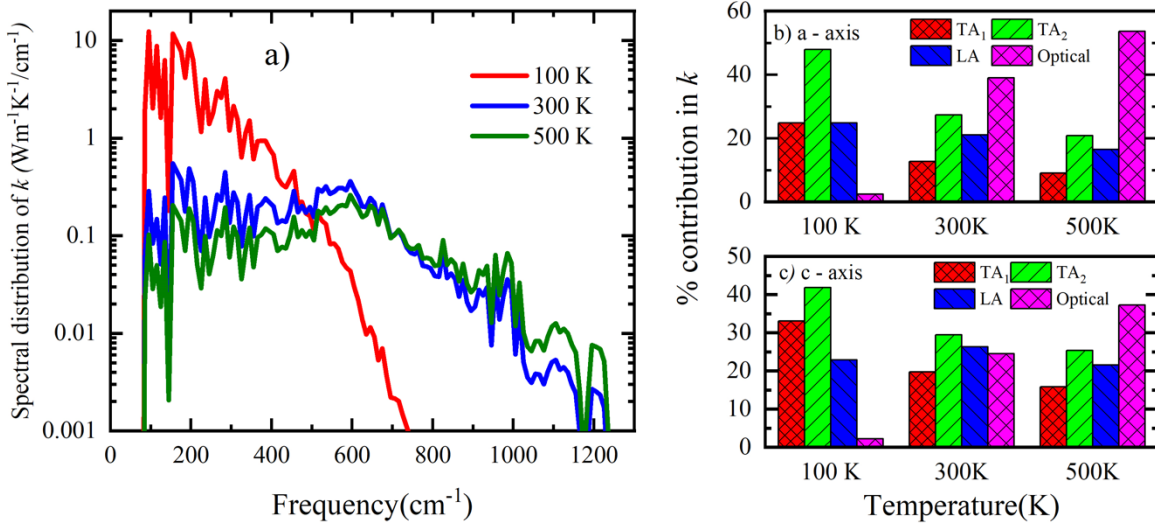


Figure 5a) Spectral distribution of k with frequency at 100 K, 300 K and 500 K. b and c) Percentage contribution by transverse acoustic (TA_1 and TA_2), longitudinal acoustic (LA) and optical phonon modes.

contribute a much higher value of ~ 95 W/mK along a-axis in BC_5 . This higher nanoscale thermal conductivity of BC_5 provides promising new avenues for achieving efficient nanoscale thermal management.

This much higher nanoscale thermal conductivity in BC_5 is found to be due to the dominant role played by optical phonons in conducting heat in BC_5 . At 500 K and 1000 K, optical phonons contribute 54% and 57.3%, respectively, to overall k along a-axis. This is in contrast to typical semiconductors like silicon, where optical phonon contribution to k is in the range of $\sim 5\%$ ²⁶ at 300 K. Large contribution of optical phonons can also be seen in Figures 5a and b which show the spectral distribution of k as well as percentage contribution of transverse acoustic (TA), longitudinal acoustic (LA) and optical phonon modes to overall k . At $T > 300$ K, optical phonons have a considerable contribution to overall thermal conductivity.

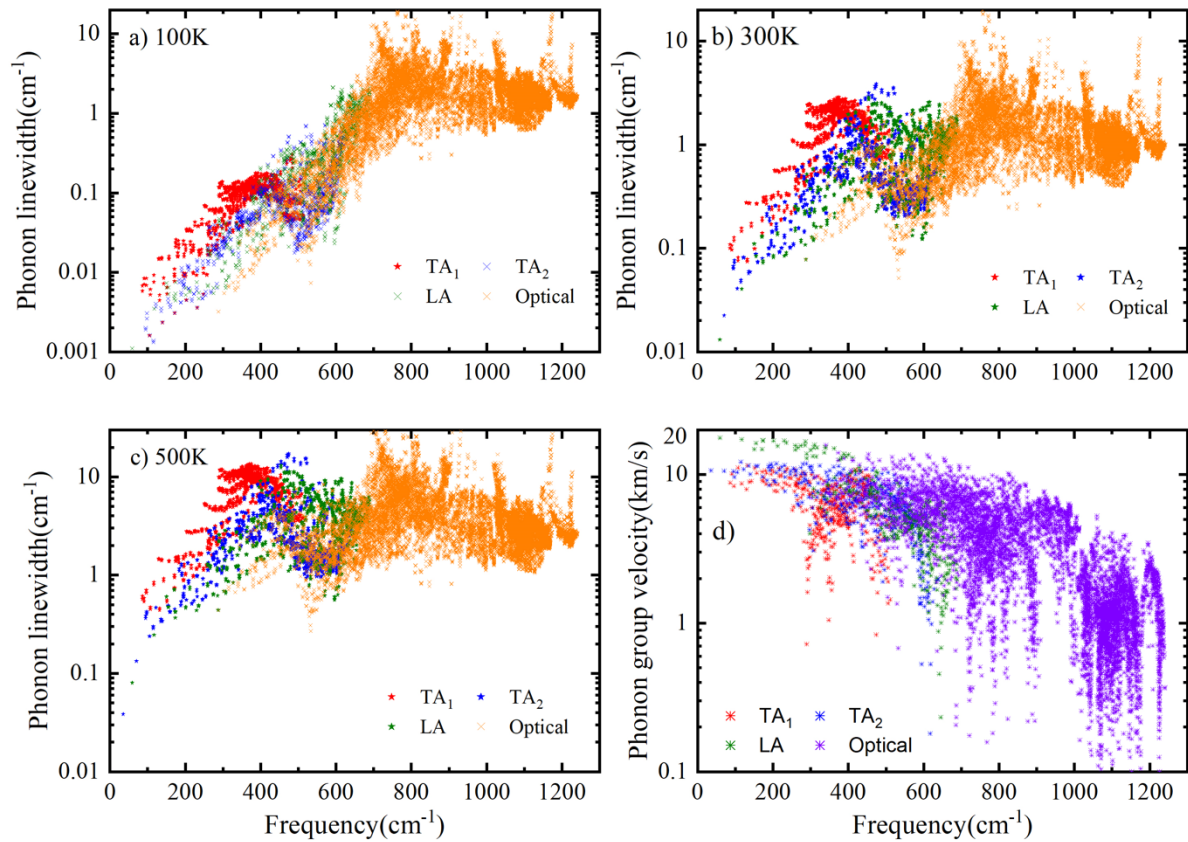


Figure 6 Phonon linewidths of transverse acoustic, longitudinal acoustic and optical phonon modes at a) 100 K b) 300 K c) 500 K. d) Phonon group velocity of all phonon modes

First-principles computations reveal that this dominant contribution of optical phonons to overall thermal conductivity in BC_5 is due to a combination of high optical phonon velocities (Fig. 6d) and comparable optical phonon scattering rates to acoustic phonons at temperatures greater than 300 K (Fig. 6a-c). This second effect is particularly interesting, since higher optical phonon frequencies typically result in optical phonon scattering rates to be significantly larger than acoustic phonons. While at 100 K, optical phonon scattering rates in BC_5 are indeed higher than acoustic phonons (Fig. 6a), as temperature increases optical-phonon scattering rates increase at a much slower rate compared to acoustic phonons, causing optical and acoustic phonon scattering rates to become comparable (Fig. 6b and c).

This weak dependence of optical phonon scattering rates on temperature and comparable scattering rates of optical and acoustic phonons in BC_5 at $T > 100$ K can be understood by observing that optical phonons in BC_5 have significantly higher frequencies than in materials like silicon. This causes optical phonons in BC_5 to scatter by decaying into phonon modes which also have high frequencies. In Fig. 7a we show the dominant contributions to scattering phase space (indicative of the number of scattering channels) of an optical phonon mode with wavevector $\mathbf{q} = (0.25, 0, 0)(2\pi/a)$ (where a is the lattice parameter) and frequency $\omega = 1021.6 \text{ cm}^{-1}$. A phonon mode with frequency ω can scatter either by an absorption process (energy conservation: $\omega + \omega' = \omega''$) or by a decay process (energy conservation: $\omega = \omega' + \omega''$) represented by the first and second delta functions in Equation 2. The x -axis of Fig. 7a corresponds to lower of the two frequencies ω' and

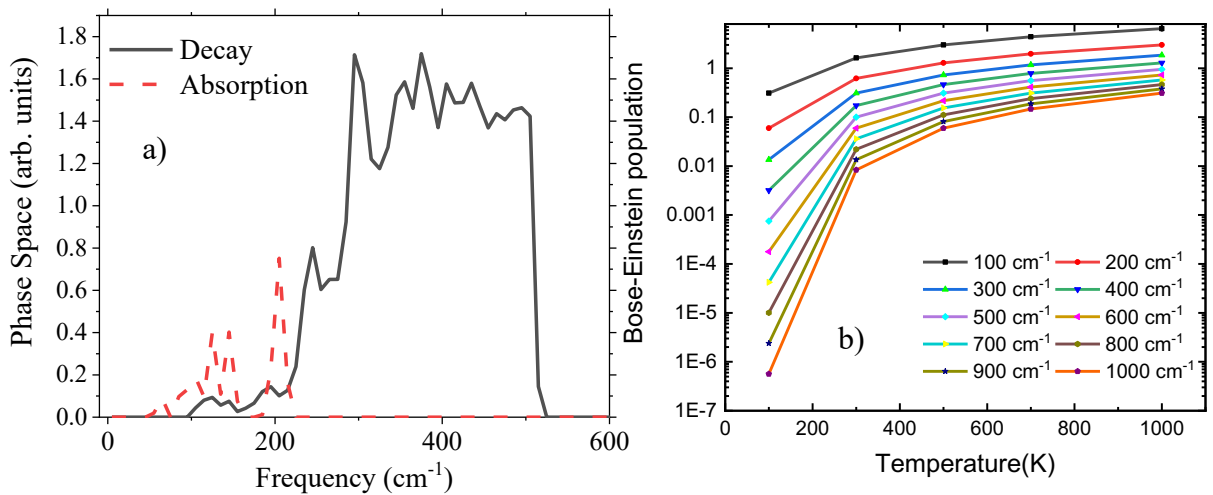


Figure 7: a) Scattering Phase space and b) Bose-Einstein population of phonons in BC_5 .

ω'' (denoted by ω' in Fig. 7a) involved in the scattering of above outlined optical phonon mode with frequency ω . The high frequency of the optical phonon (in Fig. 7a) ensures that frequencies of phonons involved in the decay channels are also high (in the range of 400 cm^{-1}). It is also clearly visible that decay channels make a large contribution to overall scattering phase space of optical phonons.

The relative insensitivity of optical phonon linewidths to temperature can now be understood by noticing that the scattering rates due to decay processes are proportional to $1 + n_{\lambda'} + n_{\lambda''}$ (second term in Equation 2). The high frequencies of the phonons ($\sim 400 \text{ cm}^{-1}$ as seen in Fig. 7a) involved in decay of optical phonons causes their populations ($n_{\lambda'}$ and $n_{\lambda''}$) to be remain less than 1.0 even as the temperature increases from 100 K to 800 K (Fig. 7b). The presence of a constant prefactor of 1 in the decay term $1 + n_{\lambda'} + n_{\lambda''}$, then ensures that the overall magnitude of the term, $1 + n_{\lambda'} + n_{\lambda''}$, does not increase significantly over the temperature range of 100 – 800 K, due to the populations, $n_{\lambda'}$ and $n_{\lambda''}$, not exceeding 1.0 over this temperature range. This causes the linewidths of optical phonons to increase slowly with temperature.

For acoustic phonons, however, the dominant scattering mechanism involves absorption scattering channels, which have a population dependence of $n_{\lambda'} - n_{\lambda''}$ (first term in Equation 2). Acoustic phonon scattering rates thus increase in direct proportion to the increase in phonon populations with temperature resulting in a strong increase in linewidths of acoustic phonons. This coupled with only a small increase in linewidths of optical phonons with increase in temperature, causes the linewidths of the two phonon modes to become comparable at temperatures of 300 K

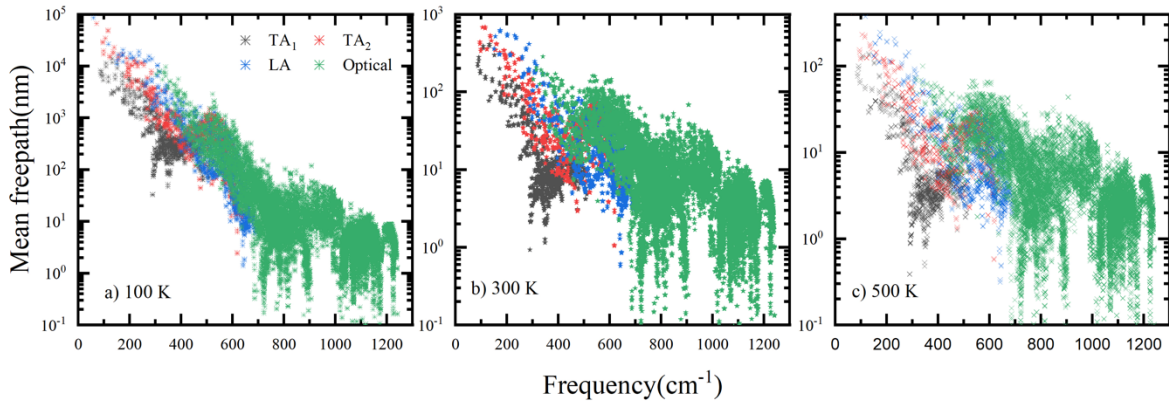


Figure 8: Phonon meanfreepaths in BC₅ at a) 100 K b) 300 K and 500 K.

and higher (Fig. 6). These results alongwith high phonon group velocities of optical phonons and a large phonon density of states of optical phonon modes at frequencies $\omega > 500 \text{ cm}^{-1}$ causes optical phonon modes to be a dominant heat carrying channel for the BC_5 system.

Optical phonon meanfreepaths in BC_5 are in the range of nanometers (tens of nanometers) as seen in Fig. 8. The large optical phonon contribution to thermal conductivity coupled with optical phonon meanfreepaths being in the nanometer regime, leads to a large contribution to k in nanoscale regime in BC_5 . Furthermore, as temperature increases to 300 K and higher, the large increase in acoustic phonon linewidths also causes their meanfreepaths to decrease to nanometers (Fig. 8), further contributing to high nanoscale k in BC_5 . k contribution from TA, LA and optical phonons for BC_5 at nanometer length of $L=100 \text{ nm}$ in comparison with silicon is discussed in supplementary information(S4).

Though the hardness of BC_5 is comparable to diamond, its thermal conductivity is much lower than diamond. The presence of large number of optical phonon branches, results in a dramatic increase in scattering phase space, resulting in phonon scattering rates being significantly larger in BC_5 than in diamond (Fig. 9). k contribution from TA, LA and optical phonons for diamond is discussed in supplementary information(S2b).

In summary, using first principles calculations, we analyzed the thermal conductivity of an ultrahard BC_5 by solving the Boltzmann transport equation exactly. At room temperature, we report a high thermal conductivity of $169 \text{ Wm}^{-1}\text{K}^{-1}$ for the bulk BC_5

and $51 \text{ Wm}^{-1}\text{K}^{-1}$ at the nanometer length scales of $L= 50 \text{ nm}$. Ultrahard BC_5 will be a promising material for thermal management due to its high thermal conductivity. We also reveal the contributions of optical phonons to overall thermal conductivity to be dominant at high temperatures. At 500 K, optical phonons contribute $\sim 54\%$ to the overall thermal conductivity. This large contribution of optical phonons to overall k was found to be due to comparable group

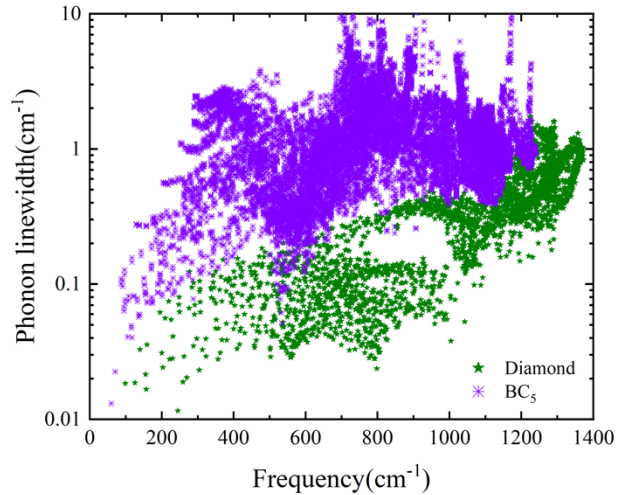


Figure 9: Phonon linewidths of BC_5 and Diamond

velocities and scattering rates to acoustic phonons at temperatures greater than 300 K. The comparable scattering rates of optical phonons arise from the particular population dependence of decay channels involved in scattering of optical phonons. The large contribution of optical phonons coupled with their meanfreepaths being in the nanometer regime leads to high nanoscale thermal conductivity in BC₅. These results may lead to potential applications of BC₅ in nanoscale thermal management.

Conflicts of Interest

There are no conflicts of interest to declare.

Acknowledgements

RM and JG acknowledge support from National Science Foundation CAREER award under Award No. #1847129. We also acknowledge OU Supercomputing Center for Education and Research (OSCER) for providing computing resources for this work.

References:

1. Senturk, A. E.; Oktem, A. S.; Konukman, A. E. S., Thermal conductivity and mechanical properties of graphene-like BC₂, BC₃ and B₄C₃. *Molecular Simulation* **2020**, *46* (12), 879-888.
2. Solozhenko, V. L.; Godec, Y. L., A Hunt for Ultrahard Materials. *Journal of Applied Physics* **2019**, *126* (23), 230401.
3. Chang, H.; Tu, K.; Zhang, X.; Zhao, J.; Zhou, X.; Zhang, H., B₄C₃ Monolayer with Impressive Electronic, Optical, and Mechanical Properties: A Potential Metal-Free Photocatalyst for CO₂ Reduction under Visible Light. *The Journal of Physical Chemistry C* **2019**, *123* (41), 25091-25101.
4. Guo, X.; He, J.; Xu, B.; Liu, Z.; Yu, D.; Tian, Y., First-Principles Investigation of Dense B₄C₃. *The Journal of Physical Chemistry C* **2007**, *111* (37), 13679-13683.
5. Gao, F.; Klug, D. D.; Tse, J. S., Theoretical study of new superhard materials: B₄C₃. *Journal of Applied Physics* **2007**, *102* (8), 084311.
6. Muthaiah, R.; Tarannum, F.; Annam, R. S.; Nayal, A. S.; Danayat, S.; Garg, J., Thermal conductivity of hexagonal BC₂P – a first-principles study. *RSC Advances* **2020**, *10* (70), 42628-42632.
7. Nayeb Sadeghi, S.; Vaez Allaei, S. M.; Zebarjadi, M.; Esfarjani, K., Ultra-high lattice thermal conductivity and the effect of pressure in superhard hexagonal BC₂N. *Journal of Materials Chemistry C* **2020**.

8. Shafique, A.; Shin, Y.-H., Ultrahigh and anisotropic thermal transport in the hybridized monolayer (BC₂N) of boron nitride and graphene: a first-principles study. *Physical Chemistry Chemical Physics* **2019**, *21* (31), 17306-17313.
9. Zhao, W. J.; Wang, Y. X., Mechanical properties of superhard diamondlike BC₅. *Solid State Communications* **2011**, *151* (6), 478-481.
10. Lazar, P.; Podloucky, R., Mechanical properties of superhard BC₅. *Applied Physics Letters* **2009**, *94* (25), 251904.
11. Ceperley, D. M.; Alder, B. J., Ground State of the Electron Gas by a Stochastic Method. *Physical Review Letters* **1980**, *45* (7), 566-569.
12. Giannozzi, P.; Baroni, S.; Bonini, N.; Calandra, M.; Car, R.; Cavazzoni, C.; Ceresoli, D.; Chiarotti, G. L.; Cococcioni, M.; Dabo, I.; Dal Corso, A.; de Gironcoli, S.; Fabris, S.; Fratesi, G.; Gebauer, R.; Gerstmann, U.; Gougoussis, C.; Kokalj, A.; Lazzeri, M.; Martin-Samos, L.; Marzari, N.; Mauri, F.; Mazzarello, R.; Paolini, S.; Pasquarello, A.; Paulatto, L.; Sbraccia, C.; Scandolo, S.; Sclauzero, G.; Seitsonen, A. P.; Smogunov, A.; Umari, P.; Wentzcovitch, R. M., QUANTUM ESPRESSO: a modular and open-source software project for quantum simulations of materials. *Journal of Physics: Condensed Matter* **2009**, *21* (39), 395502.
13. Monkhorst, H. J.; Pack, J. D., Special points for Brillouin-zone integrations. *Physical Review B* **1976**, *13* (12), 5188-5192.
14. Calandra, M.; Mauri, F., High- T_c Superconductivity in Superhard Diamondlike BC_5 . *Physical Review Letters* **2008**, *101* (1), 016401.
15. Chung, D. H.; Buessem, W. R., The Voigt-Reuss-Hill (VRH) Approximation and the Elastic Moduli of Polycrystalline ZnO, TiO₂ (Rutile), and α -Al₂O₃. *Journal of Applied Physics* **1968**, *39* (6), 2777-2782.
16. Paulatto, L.; Errea, I.; Calandra, M.; Mauri, F., First-principles calculations of phonon frequencies, lifetimes, and spectral functions from weak to strong anharmonicity: The example of palladium hydrides. *Physical Review B* **2015**, *91* (5), 054304.
17. Garg, J.; Bonini, N.; Marzari, N., First-Principles Determination of Phonon Lifetimes, Mean Free Paths, and Thermal Conductivities in Crystalline Materials: Pure Silicon and Germanium. In *Length-Scale Dependent Phonon Interactions*, Shindé, S. L.; Srivastava, G. P., Eds. Springer New York: New York, NY, 2014; pp 115-136.
18. Fugallo, G.; Lazzeri, M.; Paulatto, L.; Mauri, F., Ab initio variational approach for evaluating lattice thermal conductivity. *Physical Review B* **2013**, *88* (4), 045430.
19. Srivastava, G. P., *The Physics of Phonons*. Taylor & Francis: 1990.
20. Paulatto, L.; Mauri, F.; Lazzeri, M., Anharmonic properties from a generalized third-order ab initio approach: Theory and applications to graphite and graphene. *Physical Review B* **2013**, *87* (21), 214303.
21. Casimir, H. B. G., Note on the conduction of heat in crystals. *Physica* **1938**, *5* (6), 495-500.
22. Jain, A.; McGaughey, A. J. H., Effect of exchange–correlation on first-principles-driven lattice thermal conductivity predictions of crystalline silicon. *Computational Materials Science* **2015**, *110*, 115-120.

23. Valentin, A.; Sée, J.; Galdin-Retailleau, S.; Dollfus, P., Study of phonon modes in silicon nanocrystals using the adiabatic bond charge model. *Journal of Physics: Condensed Matter* **2008**, *20* (14), 145213.
24. Alp, I. O.; Ciftci, Y. O., Physical Properties of Superhard Diamond-Like BC5 from a First-Principles Study. *Journal of Electronic Materials* **2018**, *47* (1), 272-284.
25. Meija, J.; Coplen, T. B.; Berglund, M.; Brand, W. A.; De Bièvre, P.; Gröning, M.; Holden, N. E.; Irrgeher, J.; Loss, R. D.; Walczyk, T.; Prohaska, T., Atomic weights of the elements 2013 (IUPAC Technical Report). *Pure and Applied Chemistry* **2016**, *88* (3), 265-291.
26. Esfarjani, K.; Chen, G.; Stokes, H. T., Heat transport in silicon from first-principles calculations. *Physical Review B* **2011**, *84* (8), 085204.

Supplementary Information

Diamond:

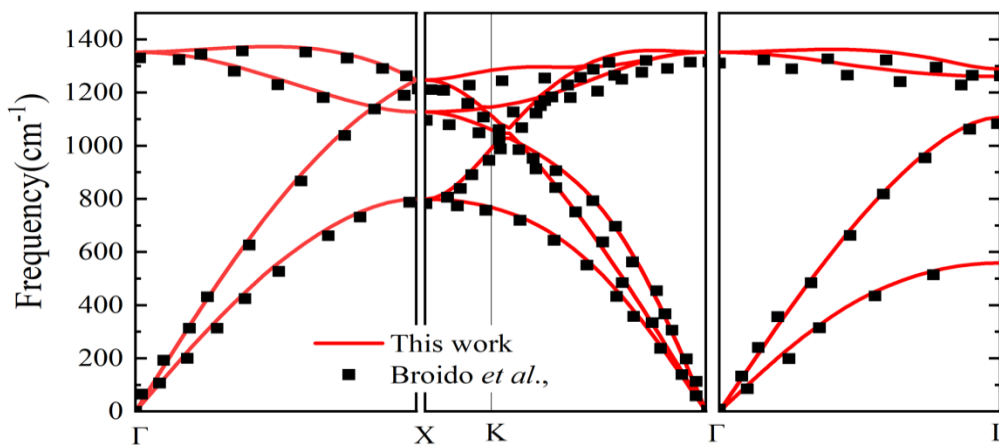


Figure S1: Phonon dispersion for the c_diamond

Figure S1 shows the phonon dispersion for the cubic diamond which are in good agreement with the previous work by Broido *et al.* work. We used the energy cut off of 70 Ry and $8 \times 8 \times 8$ k-point mesh were used to integrate the Brillouin zone. 2nd order force constants were computed on $8 \times 8 \times 8$ q-points and acoustic sum rules were imposed to the 2nd order force constants.

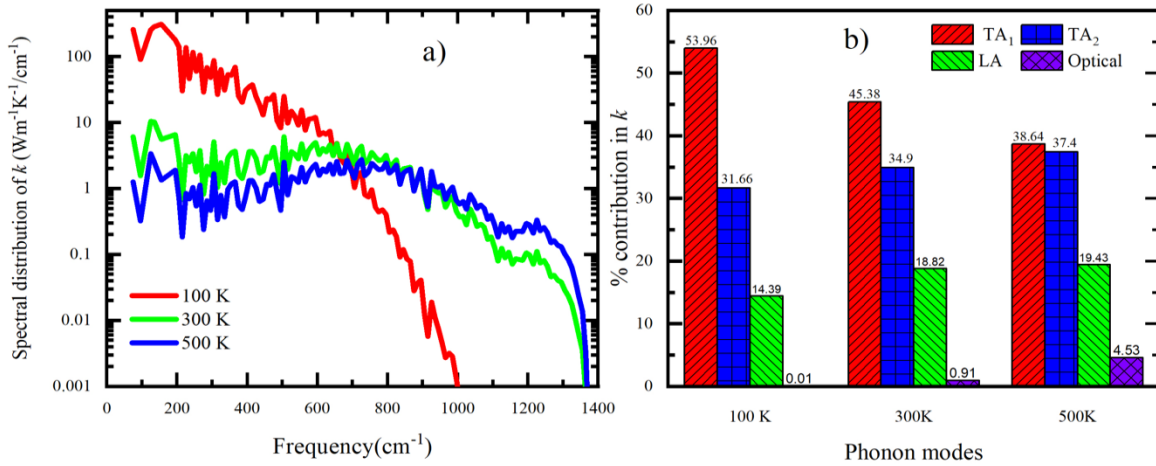


Figure S2a) Spectral distribution and b) thermal conductivity contribution from different phonon branches at 100K, 300 K and 500 K for c_Diamond.

Figure S2b represents the thermal conductivity contribution by TA, LA and optical phonon modes for the bulk cubic diamond at different temperature using SMA. We can observe that, at 500 K thermal conductivity from the optical phonons are minimal (~4.5 %) compared to 57.3% in BC₅.

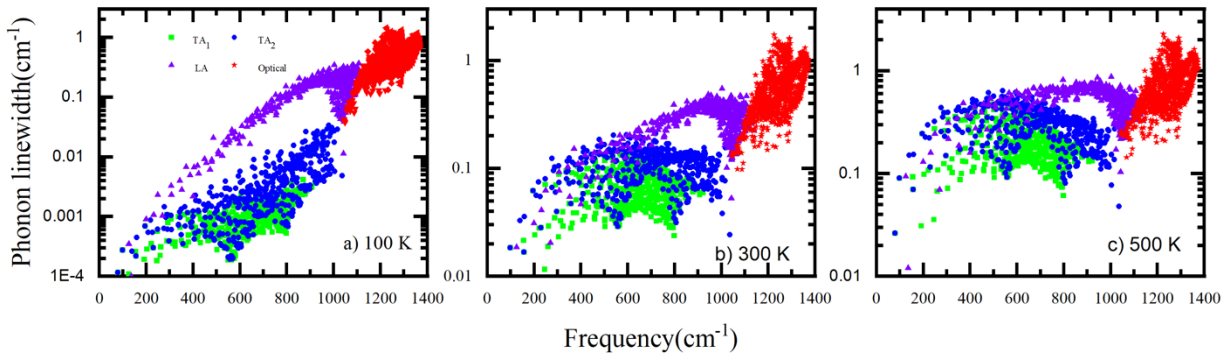


Figure S3: Phonon linewidth for the c_diamond at a)100 K, b)300 K and c)500 K.

Figure S3 shows the phonon linewidth for the cubic diamond at 100 K, 300 K and 500 K. We can observe that, optical phonons has higher scattering rate than the acoustic phonons even at high temperature(500 K).

Silicon

For silicon, we used the energy cut off of 70 Ry and $8 \times 8 \times 8$ k-point mesh were used to integrate the Brillouin zone. 2nd order force constants were computed on $8 \times 8 \times 8$ q-points and acoustic sum rules were imposed to the 2nd order force constants.

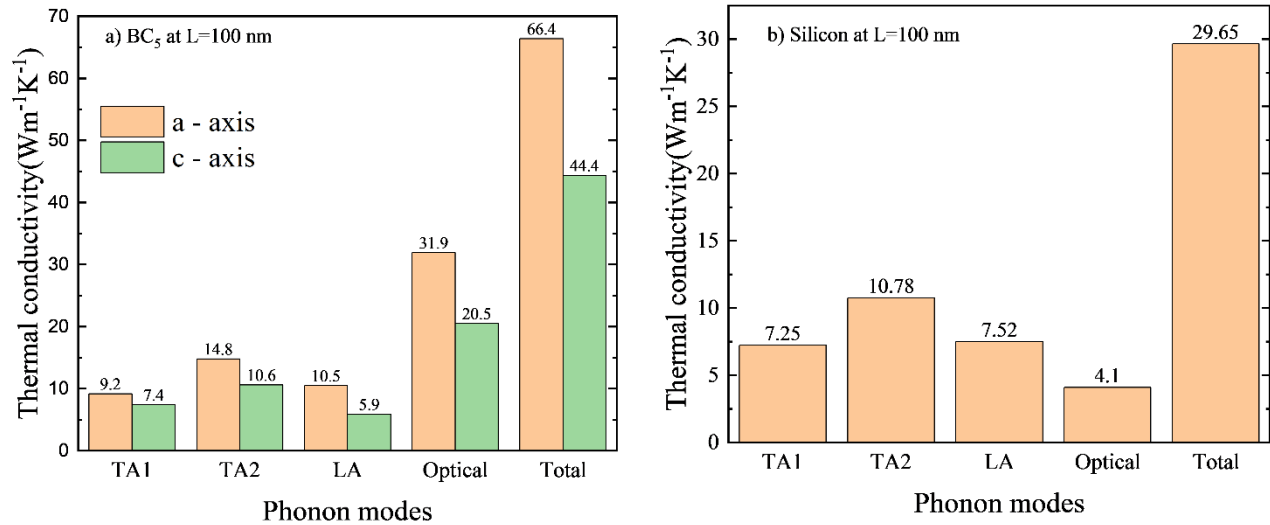


Figure S4 : Thermal conductivity contribution from TA, LA and optical phonons for BC5 and silicon at L=100 nm

Thermal conductivity(SMA) contribution from the TA, LA and optical phonon modes at nanometer length scales of L=100 nm are shown in Fig S4. We also shown the length dependence thermal conductivity of BC5 and silicon in Fig. S5 and we can observe that, at nanometer length scales, thermal conductivity of BC5 is ~120% higher than the silicon(at L=100 nm).

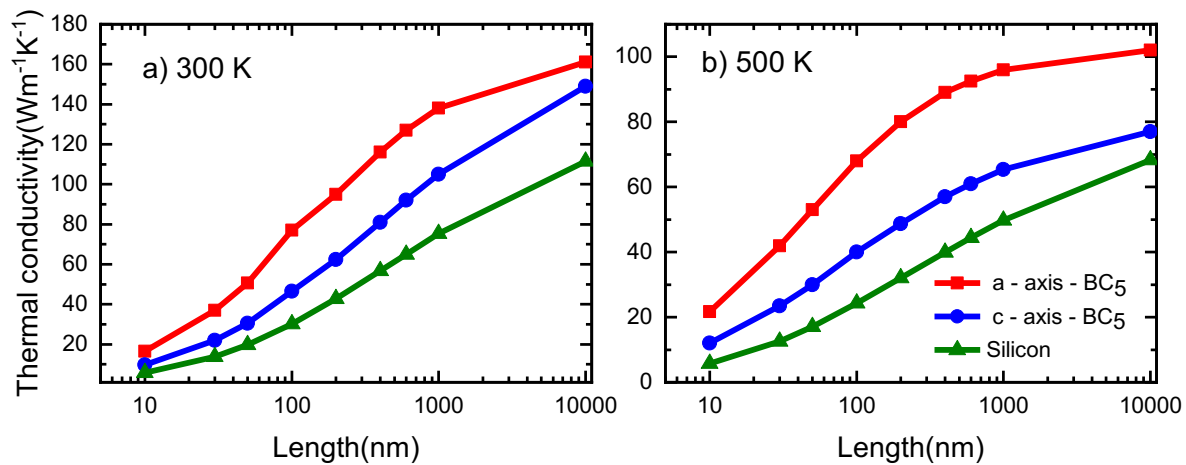


Figure S5: Length dependence thermal conductivity of BC5 and silicon at a) 300 K and 500 K